CHINESE OPTICS LETTERS

Vol. xx, No. x | April 2024

Optical Spectra of Plasmon–Exciton Core–Shell Nanoparticles: An Anisotropic Classical Model Eliminates Discrepancies with Experiments

Alexey D. Kondorskiy*

P.N. Lebedev Physical Institute of the Russian Academy of Sciences, Leninskiy prosp. 53, 119991 Moscow, Russia

***Corresponding author:** kondorskiy@lebedev.ru

Received Month X, XXXX | Accepted Month X, XXXX | Posted Online Month X, XXXX

The optical properties of the hybrid core–shell nanostructures composed of a metallic core and an organic shell of molecular J-aggregates are determined by the electromagnetic coupling between plasmons localized at the surface of the metallic core and Frenkel excitons in the shell. In cases of strong and ultra-strong plasmon–exciton coupling, the use of the traditional isotropic classical oscillator model to describe the J-aggregate permittivity may lead to drastic discrepancies between theoretical predictions and the available experimental spectra of hybrid nanoparticles. We show that these discrepancies are not caused by limitations of the classical oscillator model itself, but by considering the organic shell as an optically isotropic material. By assuming a tangential orientation of the classical oscillators of the molecular J-aggregates in a shell, we obtain excellent agreement with experimental extinction spectra of TDBC-coated gold nanorods, which cannot be treated with the conventional isotropic shell model. Our results extend the understanding of the physical effects in the optics of metal–organic nanoparticles and suggest an approach for the theoretical description of such hybrid systems.

Keywords: 160.4236 Nanomaterials, 250.5403 Plasmonics, 240.5420 Polaritons, 160.4890 Organic materials, 160.4760 Optical properties, 160.1190 Anisotropic optical materials, 290.5850 Scattering, particles

DOI: xxxxxxx/COLxxxxxxx.

1. Introduction

Studies of hybrid metal-organic nanoparticles have attracted considerable interest due to the wide range of potential applications of such structures in nanophotonics[1–6]. Because of their unique properties, core-shell nanoparticles are being exploited in a wide range of applications, including light harvesting[7–9] and light emitting devices[9,10], sensing[11,12], biotechnology[12,13], and neuromorphic optical computing[14,15]. Nanoparticles composed of a metallic core and an organic shell of ordered J- and H-aggregates of molecules are of particular interest[6,16–21]. The optical properties of such structures are determined by the electromagnetic near-field interaction between Frenkel excitons in the outer organic shell and plasmons localized at the surface of the metallic core. As the strength of this plasmon–excitonic (plexcitonic) coupling increases, the plasmonic band in the metallic core and the excitonic band in the organic shell form hybrid polariton states of the entire nanosystem with qualitatively new properties compared to those of the individual components[17]. The spectral properties of these polariton states can be controlled by tuning the parameters of the plasmonic and excitonic bands. Advances in the synthesis of plasmonic nanostructures allow the fabrication of metallic cores of different sizes and shapes with tunable plasmonic band parameters[22]. The use of molecular J-aggregates of the cyanine dye in the organic shell significantly enhances the plexcitonic coupling in the hybrid system due to the narrow and intense absorption features of these aggregates[23,24]. The size, shape and optical constants of the metallic and organic compounds of the nanoparticle determine different possible regimes of plexcitonic coupling. These regimes include weak, strong, and ultra-strong coupling, which have been extensively discussed in several review articles[1,6,17,25].

Plexcitonic systems are typically simulated using classical electromagnetic tools such as Mie theory and its extensions[26–28] or numerical Maxwell equation solvers[29]. The dielectric functions of the materials are described by the Drude-Lorentz model for the metallic core and the scalar (isotropic) classical Lorentz oscillator model for the organic shell. When the plexcitonic coupling is sufficiently strong, predictions obtained with the described classical approach are found to disagree with experimental results[30]. The discrepancy is particularly noticeable in the studies of metal-organic structures with a shell made of the J-aggregate of the TDBC dye, since the value of the reduced oscillator strength of its excitonic band is large ($f = 0.36$)[31,32]. The plexcitonic coupling energy (Rabi splitting) in the system reaches hundreds of meV. In this case, the above isotropic classical model predicts a third resonance between the two polariton bands[16,33], which is associated with an uncoupled shell mode. However, this resonance has never been observed experimentally in spectra of pure metal-organic particles with a shell of J-aggregates (see discussion in Ref.[30]), except for samples containing residual uncoupled emitters[34].

Regarding this problem, it is worthwhile to mention here some recent discussions about validity of the classical description of the nanoparticle excitonic subsystem. A remarkable number of works is devoted to the discussion of the importance of the consideration of quantum effects induced by the enhancement of the electromagnetic field in the vicinity of the metallic surface[6,17,30,31,33]. In Ref.[30] it was suggested that by considering the quantum effects one can avoid the discrepancies between the predictions of the classical model and the experimental data in the cases of strong and ultra-strong plexcitonic coupling. The heuristic quantum model introduced therein provides an expression for the frequency-dependent dielectric function of the shell material that includes the collective vacuum Rabi frequency, which depends on the size and shape of the structure. Using this model, the authors obtained excellent agreement with a series of experimental extinction spectra of metal-organic particles with different coupling strengths due to systematic size variation. To the best of our knowledge, Ref.[30] is the only work that explicitly addresses the problem of discrepancies between the predictions of the classical model and the experimental results.

In present letter, we give a completely different theoretical explanation for the discrepancies between the predictions of the isotropic classical model and the experimental results on the spectral properties of metal–organic particles with a shell made of the J-aggregates. We believe that the appearance of the uncoupled shell mode resonance in the theoretical spectra, which is not observed experimentally, is not a result of the limitation of the classical description of the optical properties of the J-aggregate as compared to the quantum description. This peak appears in the theoretical results under the assumption that the optical response of the molecular J-aggregates is isotropic, so that the frequency-dependent dielectric function of the organic shell is taken in conventional scalar form,

$$\varepsilon_{\mathrm{J}}(\omega) = \varepsilon_{\mathrm{J}}^{\infty} + \frac{f_{\mathrm{J}}\omega_{\mathrm{J}}^2}{\omega_{\mathrm{J}}^2 - \omega^2 - i\omega\gamma_{\mathrm{J}}}, \tag{1}$$

where ω_{J} is the resonance frequency of the J-band, γ_{J} is its full width, f_{J} is the reduced oscillator strength, and $\varepsilon_{\mathrm{J}}^{\infty}$ is the permittivity outside the J-band. Recently, it has been demonstrated that several experimental results for the optical spectra of metal-organic nanostructures[35–37] cannot be explained in terms of the isotropic response model. The experimental data can be well described if the anisotropic and orientational effects of the outer J-aggregate shell are taken into account in the theoretical treatment of the optical properties of hybrid metal/J-aggregate and metal/spacer/J-aggregate nanoparticles[21].

2. Theoretical approach

To confirm our statement, we perform numerical simulations of the extinction spectra of bare and J-aggregate coated gold spherical nanoparticles and nanorods considered in Ref.[30] with the dielectric function of an anisotropic molecular J-aggregate represented in tensor form with frequency dependence described by the classical Lorentz oscillator model. The theoretical approach used is described in Ref.[21].

To calculate the spectra of core-shell spherical nanoparticles, we use the formulas of the anisotropic version of Mie theory[26]. These formulas are similar to those of the original Mie theory with appropriately modified indices and arguments of the spherical Bessel functions. This similarity could be used to extend the anisotropic single core-shell theory to treat aggregate of nanoparticles using approaches[27,28].

Numerical simulations of the extinction spectra of TDBC-coated gold nanorods are performed using the FDTD method implemented in the freely available software package MIT Electromagnetic Equation Propagation (MEEP)[29]. The details of the calculation method can be found in[38]. Using the numerical method, it is possible to evaluate the cross sections for a given polarization of the incident radiation. We denote by $\sigma_{\alpha}^{(\mathrm{ext})}$ the extinction cross section obtained for the case when the electric field is directed along the α axis, with $\alpha = $ X, Y, Z (see Fig. 3d). Due to the axial symmetry of the nanorod around the Y-axis, one has $\sigma_X^{(\mathrm{ext})} = \sigma_Z^{(\mathrm{ext})}$. The final results are presented for orientationally averaged cross sections corresponding to naturally polarized light incident on the randomly oriented nanorods in colloidal solutions, $\langle \sigma^{(\mathrm{ext})} \rangle = (\sigma_Y^{(\mathrm{ext})} + 2\sigma_Z^{(\mathrm{ext})})/3$.

We assume axial symmetry of the optical properties of the molecular J-aggregate and describe the components of the dielectric function tensor of the organic shell in terms of $\varepsilon_{\parallel}$ and $\varepsilon_{\perp}$, which are the tensor components associated with the direction parallel to the aggregate orientation axis (*longitudinal* component) and perpendicular to it (*transverse* component), respectively. We assume that the TDBC J-aggregate could be described by longitudinal Lorentzian only (a general expression is discussed in[21]),

$$\begin{aligned} \varepsilon_{\parallel}(\omega) &= \varepsilon_{\mathrm{J}}^{\infty} + \frac{f_J^{\parallel}\omega_J^2}{\omega_J^2 - \omega^2 - i\omega\gamma_J}, \\ \varepsilon_{\perp}(\omega) &= \varepsilon_{\mathrm{J}}^{\infty}. \end{aligned} \tag{2}$$

This assumption is confirmed by experimental observations of the orientation-dependent optical spectra of TDBC-like aggregates, which exhibit anisotropic absorption with the strong sharp band with the dipole oriented along a single axis[39,40].

Following Ref.[21], we consider three cases of molecular arrangements in the J-aggregate shell: (I) *Normal* aggregate orientation, when the direction of the $\varepsilon_{\parallel}$ component is parallel to the normal direction to a nanoparticle surface; (II) *Tangential* aggregate orientation, in which the direction of the $\varepsilon_{\parallel}$ component is perpendicular to the normal direction, and we assume the equiprobable orientation of the aggregate axis along the tangential plane of a nanoparticle; (III) *Equiprobable* orientation of the aggregate axis in space. We describe these cases with a tensor oriented along the $\mathbf{e}_X$, $\mathbf{e}_Y$ and $\mathbf{e}_Z$ axes (see Fig. 1a and Fig. 3d). For the case of Eq. (2) the general tensor expressions are simplified and take the form of

$$\widehat{\varepsilon}(\omega)=\varepsilon_J^{\infty}\widehat{I}+\frac{\omega_J^2}{\omega_J^2-\omega^2-i\omega\gamma_J}\widehat{f}, \tag{3}$$

where $\widehat{I}$ is the unit tensor, and the reduced oscillator strength tensor, $\widehat{f}$, can be written for normal, tangential and equiprobable orientations, respectively, as

$$\widehat{f}_{\text{norm}}=\begin{pmatrix}0&0&0\\0&0&0\\0&0&f_J^{\parallel}\end{pmatrix}, \tag{4}$$

$$\widehat{f}_{\text{tang}}=\begin{pmatrix}\frac{1}{2}f_J^{\parallel}&0&0\\0&\frac{1}{2}f_J^{\parallel}&0\\0&0&0\end{pmatrix}, \tag{5}$$

$$\widehat{f}_{\text{epo}}=\begin{pmatrix}\frac{1}{3}f_J^{\parallel}&0&0\\0&\frac{1}{3}f_J^{\parallel}&0\\0&0&\frac{1}{3}f_J^{\parallel}\end{pmatrix}. \tag{6}$$

The case of equiprobable orientation (6) is equivalent to the isotropic model (1) with the oscillator strength of the single longitudinal band being three times larger than the oscillator strength of the isotropic model. To compare the results obtained with isotropic and anisotropic models, we take a certain value

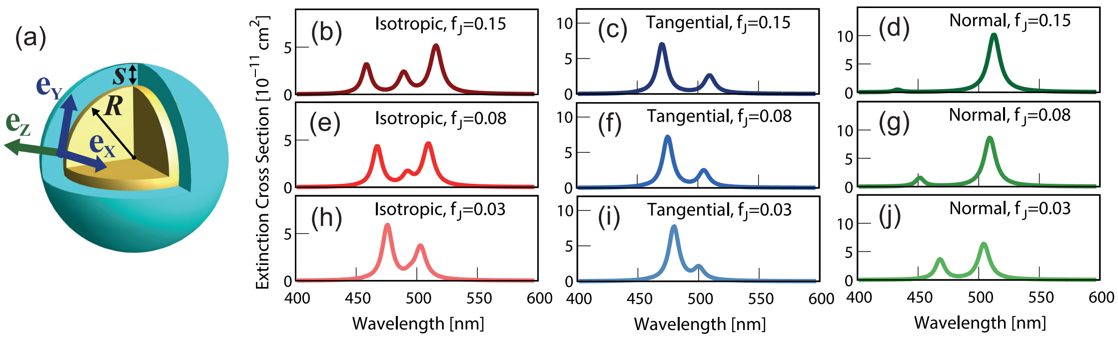

Fig. 1. (a) Schematic view of a Drude sphere with a dye shell under study. The vectors $\mathbf{e}_X$, $\mathbf{e}_Y$ and $\mathbf{e}_Z$ show the basis for the permittivity tensor of the shell material: $\mathbf{e}_Z$ is directed normal to the surface, while $\mathbf{e}_X$ and $\mathbf{e}_Y$ lie in the tangential plane. (b)–(j) Light extinction cross section of a Drude sphere with a dye shell with varying reduced oscillator strength, f_J, and different molecular arrangement in the organic shell. (b)–(d) Results are obtained for $f_J=0.15$ and: (b) *isotropic* (*equiprobable*) J-aggregate orientation, (c) *tangential* J-aggregate orientation, and (d) *normal* J-aggregate orientation in the dye shell. (e)–(g) and (h)–(j), same results calculated for $f_J=0.08$ and $f_J=0.03$, respectively .

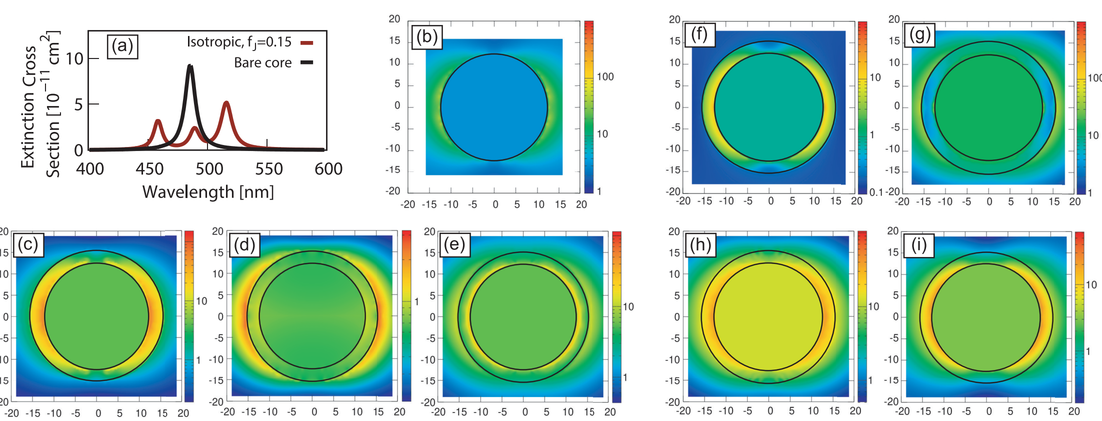

Fig. 2. (a) Light extinction cross section of a bare Drude sphere and a Drude sphere with a dye shell of *isotropic* J-aggregate orientation with $f_J=0.15$ (see Fig. 1b). (b)–(i) Electromagnetic energy density distributions in the plane lying along the light polarization and passing through the particle center. Results are presented for light wavelengths, λ, corresponding to different resonances in the light extinction spectra (see Fig. 1). (b) Bare Drude sphere, $\lambda=485$ nm. (c)–(e) Drude sphere with a dye shell with *isotropic* J-aggregate orientation: $\lambda=458$ nm (c), $\lambda=490$ nm (d) and $\lambda=517$ nm (e). (f)–(g) *normal* J-aggregate orientation: $\lambda=433$ nm (f) and $\lambda=512$ nm (g). (h)–(i) *tangential* J-aggregate orientation: $\lambda=470$ nm (h) and $\lambda=510$ nm (i). The reduced oscillator strength of a dye shell, $f_J=0.15$ for all cases. Light polarization is parallel to the horizontal axis. The color maps represent the electromagnetic energy density in the logarithmic scale.

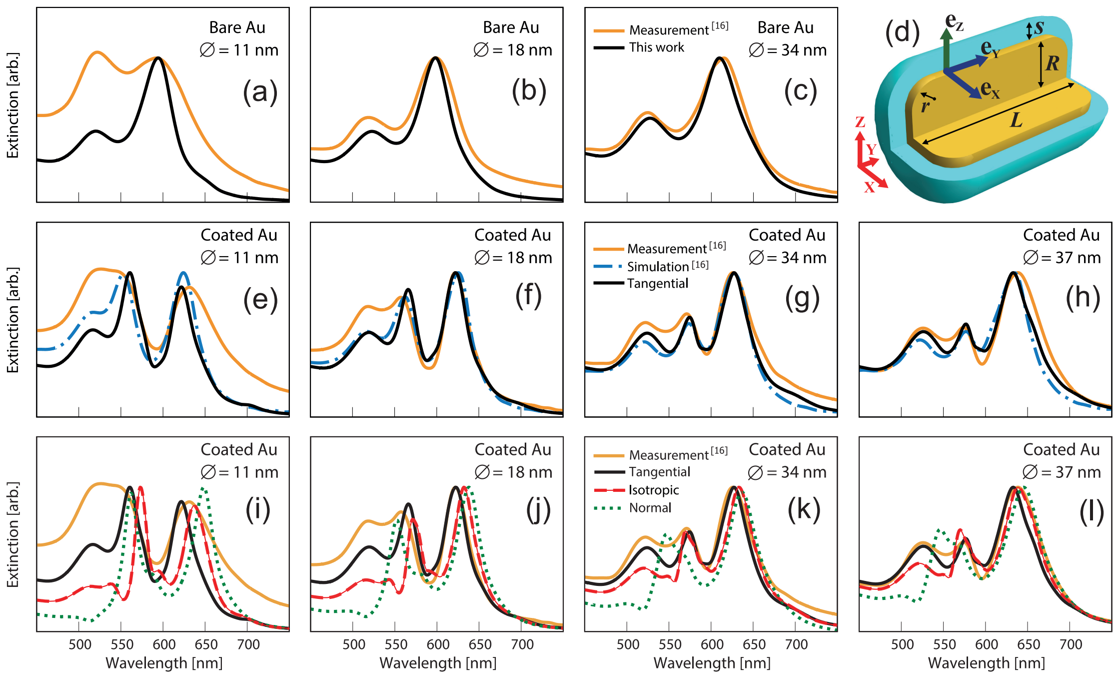

Fig. 3. (a)–(c) Light extinction spectra of bare nanorods of different sizes: (a) 11 nm, (b) 18 nm, (c) 34 nm. For the sake of brevity the results for 37 nm are not shown because they are similar to those for 34 nm. In these figures: solid orange lines – experimental results [30], solid black lines – our calculations. (d) Schematic view of a TDBC-coated gold nanorod. (e)–(h) and (i)–(l) Light extinction spectra of TDBC-coated gold nanorods of different diameters: (e) and (i) 11 nm, (f) and (j) 18 nm, (g) and (k) 34 nm, (h) and (l) 37 nm. Panels (e)–(h) show comparison of experimental results [30] (solid orange lines) and numerical simulations performed with heuristic quantum model [30] (dash-dotted blue lines) with our results obtained with classical anisotropic model for *tangential* J-aggregate orientation in the TDBC shell (solid black lines). Panels (i)–(l) show the effect of J-aggregate orientation: solid orange lines – experimental results [30], solid black lines – *tangential* orientation, thin red lines with dashes – *isotropic* (*equiprobable*) orientation, dotted green lines – *normal* orientation.

of f_J and assume that it can be estimated from the situation of the equiprobable orientations that take place in solution of the molecular aggregates. The results for normal and tangential orientations are obtained with the Eqs. (4)–(5) with $f_J^{\parallel} = 3f_J$. Because of this relation, we have a single value of f_J to refer to parameters of both the isotropic and anisotropic models used.

3. Results and discussions

First, we perform calculations of the light extinction cross section for a model Drude sphere with a dye shell in water. Our results for this system are shown in Figures 1–2. The permittivity of the core is described by the Drude model for gold, and the parameters for the permittivity of the J-aggregate shell are $\varepsilon_J^{\infty} = 1.7$, $\omega_J = 2.5$ eV, (wavelength $\lambda = 495$ nm) $\gamma_J = 0.05$ eV. The geometrical parameters are $R = 12.5$ nm and $s = 3$ nm (see Fig. 1a). The results of calculations performed with the *isotropic* classical description of the dye permittivity clearly show the growth of the uncoupled shell band around $\lambda = 490$ nm with increasing reduced oscillator strength, f_J. However, there is no such band in the results obtained with the anisotropic shell model for both the *tangential* and *normal* J-aggregate orientations in the organic shell. The electromagnetic energy density distributions around a sphere shown in Figure 2 demonstrate a significant effect of the J-aggregate orientations on the shape of the electromagnetic field spatial profile.

Second, we perform calculations of the extinction spectra of bare and TDBC-coated gold nanorods of different sizes as measured and simulated in Ref. [30]. Our results are shown in Figure 3. The notation of the sizes of the nanorods studied corresponds to the transverse diameters of 11, 18, 34, and 37 nm as measured in Ref. [30]. We use the following actual sizes of the nanorods: for a transverse diameter of 11 nm, $2R = 11.5$ nm, $L = 19.5$ nm, $r = 5$ nm; for diameter 18 nm $2R = 19.5$ nm, $L = 32$ nm, $r = 7$ nm; for diameter 34 nm $2R = 36$ nm, $L = 58$ nm, $r = 14$ nm; for diameter 37 nm $2R = 41$ nm, $L = 66$ nm, $r = 15$ nm. The permittivity of gold was taken from Ref. [41]. For bare nanorods, a 1 nm thick citrate capping layer with permittivity of 2.37 is included (see Ref. [42]). The TDBC shell thickness is $s = 3$ nm. For the TDBC J-aggregate we use the parameters of the Lorentz oscillator model, which are in agreement with those previously reported [30,32,34]: $\varepsilon_J^{\infty} = 2.3$, $\omega_J = 2.12$ eV, ($\lambda = 585$ nm) $\gamma_J = 0.048$ eV. $f_J = 0.22$. We use the same parameters of the dielectric function of the TDBC J-aggregate for all nanorod sizes in our calculations. The permittivity of the environment was set to 1.96.

Figure 3–4 shows our results for the extinction spectra of bare and TDBC-coated gold nanorods. It is seen that the results obtained for the tangential J-aggregate orientation in the organic

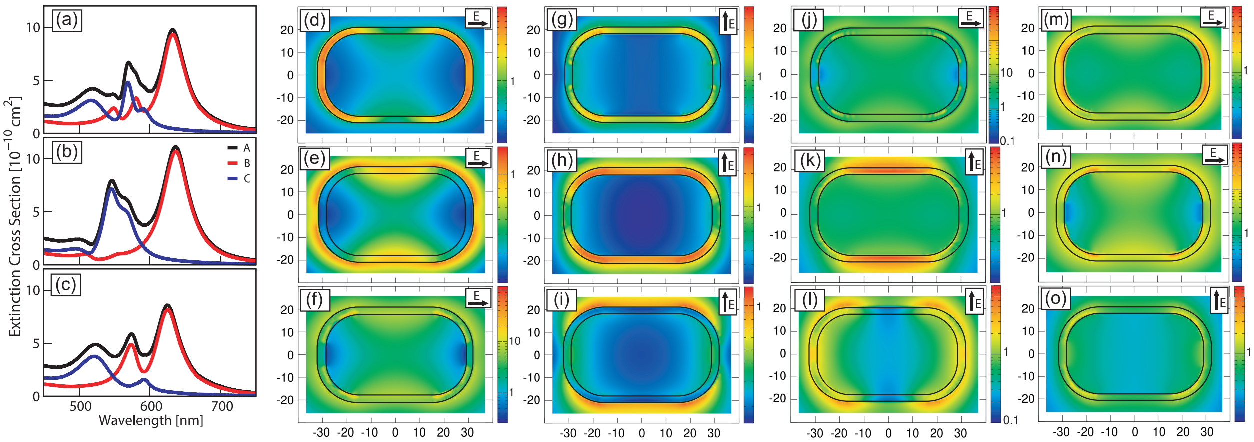

Fig. 4. (a)–(c) Light extinction cross sections of a TDBC-coated gold nanorod of size 34 nm for *isotropic* (a), *normal* (b), and *tangential* (c) J-aggregate orientations in a shell. Black curves (A) are orientation-averaged cross sections, $\langle\sigma^{(\mathrm{ext})}\rangle$. Red curves (B) and blue curves (C) are cross section contributions from cases of light polarization parallel and perpendicular to the nanorod axis, respectively (i.e. $\sigma_Y^{(\mathrm{ext})}/3$ and $2\sigma_Z^{(\mathrm{ext})}/3$). (d)–(o) Electromagnetic energy density distributions in the Y–Z plane passing through the nanorod center (see Fig. 3d). Results are presented for light wavelengths, λ, corresponding to different resonances in the light extinction spectra. (d)–(i) *isotropic* J-aggregate orientation: $\lambda = 551$ nm (d), $\lambda = 580$ nm (e), $\lambda = 635$ nm (f), $\lambda = 520$ nm (g), $\lambda = 570$ nm (h) and $\lambda = 590$ nm (i). (j)–(l) *normal* J-aggregate orientation: $\lambda = 635$ nm (j), $\lambda = 546$ nm (k) and $\lambda = 566$ nm (j). (m)–(o) *tangential* J-aggregate orientation: $\lambda = 577$ nm (m), $\lambda = 625$ nm (n) and $\lambda = 520$ nm (o). The direction of the light polarization is shown in the upper right corner of each figure. Nanorod size is 34 nm in all cases. The color maps represent the electromagnetic energy density in the logarithmic scale.

shell of the TDBC-coated gold nanorods are in good agreement with the experimental data[30]. Our calculations for the cases of isotropic (equiprobable) and normal J-aggregate orientations do not show a sufficient quality of agreement with the experimental data for all nanorod sizes. Therefore, we conclude that the J-aggregates of the TDBC dye are assembled on the metallic surface so that their axis is directed along the surface. Note that the uncoupled shell resonance appears in the spectra calculated for isotropic J-aggregate orientation around $\lambda = 585$ nm (see Figs. 3i – 3j).

The predictions of the anisotropic classical model have a similar quality of agreement with experimental data as those of the heuristic quantum model[30] (see Fig. 3). However, our model is much simpler because it does not use quantum effects. Also, this classical model does not require *ad hoc* modification of the spectroscopic parameters of the organic material due to its assembly on the metal surface, while the heuristic quantum model does. We emphasize that our theoretical results are obtained with the same set of optical parameters of the excitonic subsystem for all nanostructure sizes.

4. Conclusions

In conclusion, we report the results of theoretical studies of the optical properties of hybrid metal-organic nanoparticles with a metallic core and an organic shell made of molecular J-aggregates. We address the problem of drastic discrepancies between the theoretical predictions of the traditional isotropic classical oscillator model and some of the available experimental spectra, which appear in such systems in cases of strong and ultra-strong plasmon–exciton coupling. These discrepancies are manifested in the difference in the number of spectral bands predicted by theory and observed experimentally. The traditional classical model predicts a third resonance between the two polariton bands, which is not observed experimentally. We show that the observed discrepancies are not due to the limitations of the classical oscillator model, but to the treatment of the organic shell as optically isotropic medium.

Since optical anisotropy is an essential feature of the molecular J-aggregates, we have studied the effects of the orientation of the molecular J-aggregates in the organic shell on the optical spectra of the hybrid nanostructure. We describe anisotropic molecular J-aggregates with a dielectric function represented in tensor form with a frequency dependence described by the classical Lorentz oscillator model. We show that in the case of strong and ultra-strong plasmon–exciton coupling, the extinction spectra of the hybrid nanoparticle differ significantly for isotropic, tangential and normal orientations of the molecular J-aggregate in the organic shell. While the third peak is observed in the case of the isotropic orientation, it is not observed in either the case of the normal orientation or the tangential orientation. Furthermore, we show that the experimental extinction spectra of TDBC-coated gold nanorods[30] can be excellently reproduced if one assumes a tangential orientation of the molecular J-aggregates in shell when describing the permittivity of the J-aggregate with the use of the classical oscillator model. However, this system cannot be treated with the conventional isotropic shell model.

Our results clearly demonstrate the importance of incorporating the anisotropic optical properties of J-aggregates into the theoretical description of the optical properties of hybrid metal-organic core-shell nanostructures.

The author is grateful to V. S. Lebedev and A.A. Narits for the valuable discussions. This work was supported by the Russian Science Foundation under grant No. 19-79-30086.

References

1. E. Cao, W. Lin, M. Sun, W. Liang, and Y. Song, "Exciton-plasmon coupling interactions: from principle to applications", Nanophotonics **7**, 145 (2018).
2. J. Sun, H. Hu, D. Zheng, D. Zhang, Q. Deng, S. Zhang, and H. Xu, "Light-emitting plexciton: exploiting plasmon–exciton interaction in the intermediate coupling regime", ACS Nano, **12**, 10393 (2018).
3. D. Zheng, S. Zhang, Q. Deng, M. Kang, P. Nordlander, and H. Xu, "Manipulating coherent plasmon–exciton interaction in a single silver nanorod on monolayer WSe_2", Nano Lett. **17**, 3809 (2017).
4. J. Wen, H. Wang, W. Wang, Z. Deng, C. Zhuang, Y. Zhang, F. Liu, J. She, J. Chen, H. Chen, S. Deng, and N. Xu, "Room-temperature strong light–matter interaction with active control in single plasmonic nanorod coupled with two-dimensional atomic crystals", Nano Lett. **17**, 4689 (2017).
5. H. Chen, L. Shao, K. C. Woo, J. Wang, and H.-Q. Lin, "Plasmonic–molecular resonance coupling: plasmonic splitting versus energy transfer", J. Phys. Chem. C **116**, 14088 (2012).
6. X. Li, L. Zhou, Z. Hao, and Q.-Q. Wang, "Plasmon-exciton coupling in complex systems", Adv. Opt. Mater. **6**, 1800275 (2018).
7. S. Manzhos, G. Giorgi, J. Lüder, and M. Ihara, "Modeling of plasmonic properties of nanostructures for next generation solar cells and beyond", Advances in Physics: X, **6**, 1908848 (2021).
8. S. R. Mirnaziry, M. A. Shameli, and L. Yousefi, "Design and analysis of multi-layer silicon nanoparticle solar cells", Sci. Rep. **12**, 13259 (2022).
9. A. P. Manuel, A. Kirkey, N. Mahdi, and K. Shankar, "Plexcitonics – fundamental principles and optoelectronic applications", J. Mater. Chem. C **7**, 1821 (2019).
10. J. Perego, C. X. Bezuidenhout, I. Villa, et. al., "Highly luminescent scintillating hetero-ligand MOF nanocrystals with engineered Stokes shift for photonic applications", Nat. Commun. **13**, 3504 (2022).
11. A. Firoozi, A. Amphawan, R. Khordad, et. al., "Effect of nanoshell geometries, sizes, and quantum emitter parameters on the sensitivity of plasmon-exciton hybrid nanoshells for sensing application", Sci. Rep. **13**, 11325 (2023).
12. Y. Kim, A. Barulin, S. Kim, L. P. Lee, and I. Kim, "Recent advances in quantum nanophotonics: plexcitonic and vibro-polaritonic strong coupling and its biomedical and chemical applications", Nanophotonics **12**, 413 (2023).
13. Y. Mantri, and J. V. Jokerst, "Engineering Plasmonic Nanoparticles for Enhanced Photoacoustic Imaging", ACS Nano **14**, 9408 (2020).
14. S. Kim, N. Kim, J. Seo, et. al., "Nanoparticle-based computing architecture for nanoparticle neural networks", Sci. Adv. **6**, eabb3348 (2020).
15. G. Vats, B. Hodges, A. J. Ferguson, L. M. Wheeler, and J. L. Blackburn, "Optical Memory, Switching, and Neuromorphic Functionality in Metal Halide Perovskite Materials and Devices", Adv. Mater. **35**, 2205459. (2023).
16. V. S. Lebedev, and A. S. Medvedev, "Plasmon – exciton coupling effects in light absorption and scattering by metal/J-aggregate bilayer nanoparticles", Quantum Electron., **42**, 701 (2012).
17. P. Törmä, and W. L. Barnes, "Strong coupling between surface plasmon polaritons and emitters: a review", Rep. Prog. Phys. **78**, 013901 (2015).
18. S. Balci, "Ultrastrong plasmon–exciton coupling in metal nanoprisms with J-aggregates", Opt. Lett. **38**, 4498 (2013).
19. B. G. DeLacy, W. Qiu, M. Soljačić, C. W. Hsu, O. D. Miller, S. G. Johnson, and J. D. Joannopoulos, "Layer-by-layer self-assembly of plexcitonic nanoparticles", Opt. Express **21**, 019103 (2013).
20. A. D. Kondorskiy, and V. S. Lebedev, "Spectral-band replication phenomenon in a single pair of hybrid metal-organic nanospheres and nanodisks caused by plexcitonic coupling", Opt. Express **27**, 11783 (2019).
21. A. D. Kondorskiy, S. S. Moritaka, and V. S. Lebedev, "Manifestation of the anisotropic properties of the molecular J-aggregate shell in the optical spectra of plexcitonic nanoparticles", Opt. Express **30**, 4600 (2022).
22. N. Jiang, X. Zhuo, and J. Wang, "Active plasmonics: principles, structures, and applications", Chem. Rev. **118**, 3054–3099 (2018).
23. F. Würthner, T. E. Kaiser, and C. R. Saha-Möller, "J-Aggregates: From Serendipitous Discovery to Supramolecular Engineering of Functional Dye Materials", Angew. Chem. Int. Ed. **50**, 3376 (2011).
24. B. I. Shapiro, A. D. Nekrasov, V. S. Krivobok, and V. S. Lebedev, "Optical properties of molecular nanocrystals consisting of J-aggregates of anionic and cationic cyanine dyes", Opt. Express **26**, 30324 (2018).
25. V. Krivenkov, S. Goncharov, I. Nabiev, and Y. P. Rakovich, "Induced transparency in plasmon-exciton nanostructures for sensing applications", Laser Photonics Rev. **13**, 1800176 (2019).
26. C. Qiu, L. Gao, J. Joannopoulos, and M. Soljacic, "Light scattering from anisotropic particles: propagation, localization, and nonlinearity", Laser Photonics Rev. **4**, 268 (2009).
27. Y.-L. Xu, "Electromagnetic scattering by an aggregate of spheres", Appl. Opt. **34**, 4573 (1995).
28. M. A. Shameli, S. R. Mirnaziry, and L. Yousefi, "Distributed silicon nanoparticles: an efficient light trapping platform toward ultrathin-film photovoltaics", Opt. Express **29**, 28037 (2021).
29. https://meep.readthedocs.io.
30. F. Stete, W. Koopman, C. Henkel, O. Benson, G. Kewes, and M. Bargheer, "Optical Spectra of Plasmon–Exciton Core–Shell Nanoparticles: A Heuristic Quantum Approach", ACS Photonics **10**, 2511 (2023).
31. M. J. Gentile, S. A. Horsley, and W. L. Barnes, "Localized exciton–polariton modes in dye-doped nanospheres: a quantum approach", J. Opt. **18**, 015001 (2016).
32. M. J. Gentile, S. Núñez-Sánchez, W. L. Barnes, "Optical Field–Enhancement and Subwavelength Field–Confinement Using Excitonic Nanostructures", Nano Lett. **14**, 2339 (2014).
33. T. J. Antosiewicz, S. P. Apell, and T. Shegai,"Plasmon–Exciton Interactions in a Core–Shell Geometry: From Enhanced Absorption to Strong Coupling", ACS Photonics **1**, 454 (2014).
34. J. Bellessa, C. Symonds, K. Vynck, A. Lemaitre, A. Brioude, L. Beaur, J. C. Plenet, P. Viste, D. Felbacq, E. Cambril, and P. Valvin, "Giant Rabi splitting between localized mixed plasmon-exciton states in a two-dimensional array of nanosize metallic disks in an organic semiconductor", Phys. Rev. B **80**, 033303 (2009).
35. T. Uwada, R. Toyota, H. Masuhara, and T. Asahi, "Single Particle Spectroscopic Investigation on the Interaction between Exciton Transition of Cyanine Dye J-Aggregates and Localized Surface Plasmon Polarization of Gold Nanoparticles", J. Phys. Chem. C **111**, 1549 (2007).
36. A. Yoshida, Y.'Yonezawa, and N. Kometani, "Tuning of the Spectroscopic Properties of Composite Nanoparticles by the Insertion of a Spacer Layer: Effect of Exciton–Plasmon Coupling", Langmuir **25**, 6683 (2009).
37. N. Takeshima, K. Sugawa, H. Tahara, S. Jin, M. Noguchi, Y. Hayakawa, Y. Yamakawa, and J. Otsuki, "Combined Use of Anisotropic Silver Nanoprisms with Different Aspect Ratios for Multi–Mode Plasmon–Exciton Coupling", Nanoscale Res. Lett. **15**, 15 (2020).
38. A. D. Kondorskiy, N. T. Lam, and V. S. Lebedev, "Absorption and Scattering of Light by Silver and Gold Nanodisks and Nanoprisms", J. Russ. Laser Res. **39**, 56 (2018).
39. C. Didraga, A. Pugžlys, P. R. Hania, H. von Berlepsch, K. Duppen, and J. Knoester, "Structure, Spectroscopy, and Microscopic Model of Tubular Carbocyanine Dye Aggregates", J. Phys. Chem. B **108**, 14976 (2004).
40. A. Pugzlys, P. R. Hania, R. Augulis, K. Duppen, and P. H. M. van Loosdrecht, "Cylindrical Aggregates of 5,5',6,6'-Tetrachlorobenzimida-carbocyanine Amphiphilic Derivatives: Structure–Related Optical Properties and Exciton Dynamics", Int. J. Photoenergy **2006**, 029623 (2006).
41. R. L. Olmon, B. Slovick, T. W. Johnson, D. Shelton, S.-H. Oh, G. D. Boreman, and M. B. Raschke, "Optical dielectric function of gold", Phys. Rev. B **86**, 235147 (2012).
42. J.-W. Park, and J. S. Shumaker-Parry, "Structural Study of Citrate Layers on Gold Nanoparticles: Role of Intermolecular Interactions in Stabilizing Nanoparticles", J. Am. Chem. Soc. **136**, 1907 (2014).